THE JOURNAL OF PHYSICAL CHEMISTRY Letters

pubs.acs.org/JPCL

Distinct Infrared Spectral Signatures of the 1,2- and 1,4-Fluorinated Single-Walled Carbon Nanotubes: A Molecular Dynamics Study

Akira Ueta,[†] Yoshitaka Tanimura,[†] and Oleg V. Prezhdo*,[‡]

[†]Department of Chemistry, Graduate School of Science, Kyoto University, Kitashirakawa, Sakyoku, Kyoto 606-8502, Japan, and [‡]Department of Chemistry, University of Washington, Seattle, Washington 98195-1700

ABSTRACT Fluorinated single-walled carbon nanotubes (F-SWNTs) form important intermediates in SWNT sidewall functionalization, leading to a variety of materials and biological applications. By simulating the infrared (IR) signals for the 1,2- and 1,4-addition structures, in which fluorine atoms are arranged in ortho or para positions, respectively, on the aromatic skeleton of the (10,10) SWNT surface, we identify peaks that are unique to each structure. Our full molecular dynamics simulations show that the [−C(sp^3)−C(sp^3)−] collective vibrational peak at 400 cm^{-1} is optically active only in the 1,2-isomer, while the 1300 cm^{-1} band arising due to the F−C(sp^3) stretching motion coupled with the neighboring C(sp^2) atoms is seen in the IR spectrum of only the 1,4-isomer. The reported results suggest simple and clear experimental means for distinguishing between the two fluorinated structures and provide a valuable tool for controlled SWNT sidewall functionalization.

SECTION Nanoparticles and Nanostructures

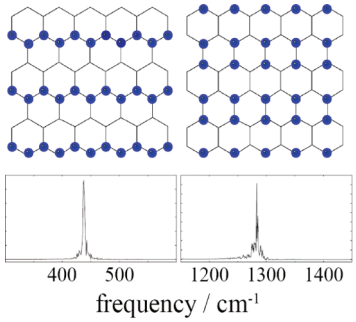

The discovery of carbon nanotubes (CNTs)[1] has led to an explosion of studies focusing on understanding and controlling CNT atomic and electronic properties, as motivated by a variety of electronics,[2−13] biological,[14−17] materials,[18−24] energy,[25−27] and other applications. Chemical functionalization of CNT sidewalls provides one of the most efficient routes to the desired property control. Examples are abundant. Addition of fluorinated olefins and chlorine atoms represents an effective approach toward converting commercial mixtures of metallic and semiconducting CNTs into high-mobility semiconducting tubes.[2,3] Functionalization with carboxylic acid, nitroso, and maleic anhydride groups allows one to control CNT charging.[5,6] The CNT optical properties can be selectively modified by fluorination.[7] Functionalization and bioconjugation of CNTs have led to multiple protocols for biomedical applications, including biological imaging, labeling, sensing, and drug delivery.[14−16] Key biological advantages of functionalized carbon nanotubes include their excellent ability to translocate through membranes while retaining low toxicity.[17] Fluoride atoms and other substituents on the CNT surface can be used to transform CNT films between the superhydrophobic and nearly hydrophilic states.[18,19] Control of surface adsorption properties by covalent and noncovalent CNT functionalization[20] leads to superior CNT−polymer composites,[21] materials with improved friction properties,[22] and strongly interconnected CNT blocks.[24] Fluorination and defluorination reactions form the basis for CNT applications in hydrogen storage[26] and Li ion batteries.[25] Finally, complexation of CNTs with organic sensitizers leads to promising photovoltaic materials.[27]

Generally, CNTs are chemically nonreactive and are hard to functionalize due to the efficient carbon−carbon bonding. The strong reactivity of fluorine atoms makes fluorination one of the most effective methods to modify and control physical−chemical properties of carbon materials.[28,29] Using technology developed for the fluorination of graphite,[30] Mickelson et al. produced fluorinated single-walled carbon nanotubes (F-SWNTs), which serve as a staging point of chemical modification for a wide variety of sidewall functionalizations.[31] The structures of F-SWNT were investigated by various methods involving infrared (IR) and Raman spectroscopies,[29,32,33] nuclear magnetic resonance (NMR),[33,34] transmission electron microscopy (TEM),[29] scanning tunneling microscopy (STM),[35] electron energy loss spectroscopy (EELS),[36] and X-ray photoemission spectroscopy (XPS).[37,38]

Despite strong synthetic efforts as well as extensive experimental and computational characterization of the fluorinated structures, the most favorable pattern of fluorine atom addition remains controversial.[28] Both 1,2-addition and 1,4-addition patterns have been proposed. The fluorine atoms (the blue balls) are arranged in ortho positions in the 1,2-isomer, while the 1,4-addition puts the atoms in para positions, as illustrated in Figure 1.[35,39,40]

While the former pattern was predicted to be more stable in the semiempirical calculation,[35] the latter pattern was

Received Date: February 2, 2010
Accepted Date: March 30, 2010

DOI: 10.1021/jz100143z | *J. Phys. Chem. Lett.* **2010**, *1*, 1307–1311

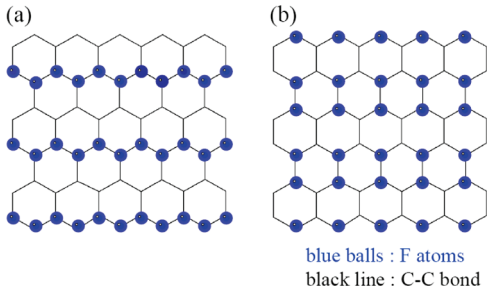

Figure 1. Two addition structures of fluorinated carbon nanotubes. (a) The 1,2-addition; (b) 1,4-addition. In each structure, blue balls depict fluorine atoms.

found to be more favorable in the DFT calculations.[41] In each case, the energy difference between the two patterns was quite small, implying that both types of fluorinated materials probably coexist.[28]

The purpose of this study is to distinguish between the 1,2- and 1,4-addition structures of F-SWNTs by means of IR spectroscopy. In order to explore this prospect, we employ classical molecular dynamics (MD)[42−45] and directly calculate the IR response function.[44−47] Our study shows that each structure can be identified by distinct IR peaks. In particular, an optically active band appears at 400 cm^{-1} in the 1,2-addition product due to collective vibrational motions involving the [−C(sp^3)−C(sp^3)−] bond created by the 1,2-addition. No equivalent band is seen in the IR spectrum of the 1,4-product. On the other hand, a 1300 cm^{-1} band originating from the F−C(sp^3) stretching motion is seen in the IR spectrum of the 1,4-isomer but not that of the 1,2-isomer.

In the following, we explain the methodology of the IR response analysis by means of MD simulation. Then, we present and discuss the calculated IR spectra for the 1,2- and 1,4-F-SWNT addition structures.

Pristine CNTs have 15 or 16 vibrational modes that are active in the Raman spectrum.[48] The corresponding IR signal is very weak since the first-order IR optical response depends on the transition dipole moment, which is practically nonexistent in ideal CNTs. Fluorine atoms break the CNT symmetry, create local dipoles, and generate an IR signal. The fluorine atoms and the sp^3 carbons generated by the fluorine addition affect the CNTs modes. The vibrational frequencies of F-SWNTs are generally higher than those of pristine CNTs. The optical response function calculated within the MD approach allows us to obtain the entire IR spectrum of F-SWNTs. In order to compare and distinguish between the two isomers, we concentrate on the C−F vibrational modes. Although fluorination changes the properties of the modes associated with the original C(sp^2) atoms, these changes are quite complicated and will not be discussed here since the analysis of the C(sp^3)−F motions already gives the desired result.

We consider the dipole correlation function $\langle \mu(t)\mu(0)\rangle$ that is obtained from the MD simulation, where $\mu(t)$ is the dipole moment of the F-SWNT system. The Fourier transform of the correlation function is defined as

$$I_{MD}(\omega) = \frac{1}{2\pi}\int_{-\infty}^{\infty} dt\, e^{-i\omega t}\langle \mu(t)\mu(0)\rangle \qquad (1)$$

While the IR spectrum $\alpha(\omega)$ is determined more rigorously via the quantum mechanical commutator $\langle[\mu(t),\mu(0)]\rangle$, the spectrum is well-approximated using the classical result $I_{MD}(\omega)$ and the harmonic assumption by

$$\alpha(\omega) \propto \omega \tanh\left(\frac{\hbar\omega}{2k_B T}\right) I_{MD}(\omega) \qquad (2)$$

Here, k_B is the Boltzmann constant, T is temperature, and $\hbar$ is Planck's constant.[46,49]

The F-SWNT MD was generated using the Amber potentials for the intramolecular C−C, C−F, and F−F interactions. In particular, the C(sp^2) atoms were assigned the "CA" Amber atom type, while C(sp^3) atoms were described using the Amber "CT" atom type.[50] Previously, the Amber force field was used in order to describe the IR spectra of peptides[44,45] and many other systems. The interactions between the atoms that were not directly bonded to each other were described by the Coulomb and van der Waals (VDW) terms. To simplify the calculation, the VDW interactions between atoms separated by more than 5 Å were disregarded. The velocity Verlet algorithm was adopted to integrate the equation of motion with a 0.1 fs time step. The simulations were performed at 300 K.

Note that classical MD does not necessarily give a very precise description of the structure and dynamics of F-SWNT due to the phenomenological interaction potential. However, the approach is sufficiently accurate to establish the differences in the IR signals for the two distinct F-SWNT isomers.

The study was performed using the (10,10) metallic armchair SWNT. Periodic boundary conditions along the tube axis were used. The simulation cell was 2.4 nm long, containing 10 benzene rings in the periodic direction. The fluorine atoms were arranged to form the 1,2- and 1,4-addition structures shown in Figure 1a and b. In both structures, all possible addition sites of the outside surface of the tube were occupied by fluorine atoms.[51] We ran MD simulations to equilibrate the system under the given conditions and checked the accuracy of the simulated structures.

In order to calculate the IR signal, the dipole moments associated with the C−F bonds were determined. The charges on the fluorine and carbon atoms were calculated quantum mechanically for a single graphene sheet with the fluorine atoms arranged as in Figure 1. The ab initio density functional theory (DFT) calculations were done using the GAMESS package, the B3LYP exchange-correlation function, and the SVP basis set. The charges were computed using the CHELPG method. We found that the bonded fluorine and carbon atoms had nearly opposite charges of about −0.2e and +0.2e, while the remaining carbon atoms were almost neutral. Further, we calculated the changes in the point charges associated with the thermal fluctuations of the C−F bond. In our MD trajectory, the bond length fluctuated within 0.1 Å of its equilibrium value, and the corresponding changes in the atomic charges calculated by DFT were small. These results indicated that the dipole moments associated with the C−F modes were directly proportional to the corresponding bond lengths.

Two independent polarizations of light were considered in detail, corresponding to the directions along the tube axis and

DOI: 10.1021/jz100143z | J. Phys. Chem. Lett. 2010, 1, 1307–1311

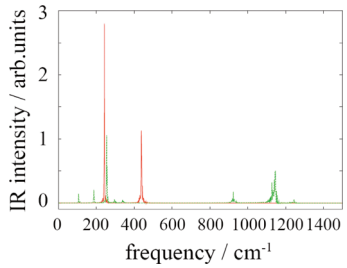

Figure 2. IR spectra of a 1,2-fluorinated carbon nanotube obtained from full MD simulations. The red solid line represents light polarization along the tube axis, whereas the green dotted line corresponds to radially polarized light.

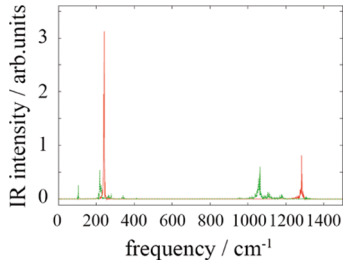

Figure 3. Same as Figure 2, but for the 1,4-fluorinated CNT.

its radius. Circularly polarized light was considered as well. Each IR response function, eqs 1 and 2, was computed by averaging over an ensemble of 10^6 initial configurations. Figures 2 and 3 display the IR spectra of the F-SWNT for light polarized along the tube axis and its radius, respectively.

Significant differences between the 1,2- and 1,4-addition structures are seen at 400 and 1300 cm^{-1}. The peak at 400 cm^{-1} is optically active only in the 1,2-addition product, whereas the peak at 1300 cm^{-1} appears only in the 1,4-isomer. In order to elucidate the atomistic origin of these and other peaks, we performed a normal-mode analysis of the F-SWNT systems. The results showed that peaks with frequencies less than 500 cm^{-1} arose from collective vibrational motions of the SWNT, while peaks with frequencies above 900 cm^{-1} were derived from local modes. The peaks corresponding to the local C−C and C−F bond vibrations produced by the Amber force field emerge within the 1100−1500 cm^{-1} frequency range. In particular, the C−F bond stretching modes appear at about 1200−1300 cm^{-1}.

In order to analyze the positions and origins of the peaks in the IR spectra, we repeated the calculations using various constraints. We fixed the positions of all sp^2 carbon atoms, neglected electrostatic and VDW interactions between fluorine atoms, and so forth. We found that the peak at around 200 cm^{-1} originated from the VDW interactions between the carbon and fluorine atoms. This peak is optically active for light polarized along both the tube axis and its radius. Since it did not depend on the electrostatic interactions involving fluorine atoms, the peak appeared in both 1,2- and 1,4-structures. Other spectral features in the 100−300 cm^{-1} range were due to CNT radial breathing modes (RBM). As a result, they were optically active only for the radially polarized light.

The peaks in the 350−400 cm^{-1} frequency range appeared in both fluorine addition structures for the radially polarized light. At the same time, they were optically active only in the 1,2-isomer for light polarized along the tube axis. These peaks originated from vibrational motions of the $C(sp^2)$ and $C(sp^3)$ atoms along and perpendicular to the tube axis. In particular, the peaks in the radially polarized spectra for both F-SWNT isomers were from the $[-C(sp^3)-C(sp^2)-]$ vibrational motions, whereas the 350−400 cm^{-1} features in the spectrum of the 1,2-addition structure for light polarized along the tube axis were attributed to the $[-C(sp^3)-C(sp^3)-]$ vibrational modes. The corresponding motions along the tube axis in the 1, 4-structure arose from the $[-C(sp^3)-C(sp^2)-C(sp^2)-C(sp^3)-]$ fragments. They had lower frequencies and did not appear in the 350−400 cm^{-1} range.

The peaks due to $F-C(sp^3)$ stretching peaks were in the 1200−1300 cm^{-1} frequency range. For the light polarized along the tube axis, the distinct peak at 1300 cm^{-1} was observed only in the 1,4-isomer. For radially polarized light, small peaks in the 1200−1300 cm^{-1} frequency range were observed in both structures. The remaining 900 and 1100 cm^{-1} peaks detectable in the IR spectrum arose from the wagging motions of the C−F bonds and the stretching motions of the $C(sp^3)-C(sp^2)$ bonds, respectively.

In addition to light polarized along the tube axis and radially polarized light, we computed the IR spectra for circularly polarized light. The results were very similar to the spectra shown in Figures 2 and 3, and therefore, they are not discussed here. No vibrational modes that were specific to the circularly polarized light were detected, at least for the (10,10) F-SWNTs.

It is instructive to comment on the relaxation mechanism for the C−F vibrational energy deposited by the IR radiation. Since the (10,10) SWNT is metallic, one may expect relaxation that is similar to the relaxation of vibrational modes of species adsorbed on bulk metal surfaces. The presence of a highly polarizable electron cloud in a bulk metal leads to the so-called "dynamic dipole mechanism" [52], in which the fluctuations in the dipole moment of the vibrational mode, in our case the C−F bond, couple to the electronic degrees of freedom of the substrate. Our calculations indicate that the dynamic dipole mechanism plays little role in SWNTs. The charges on the carbon atoms that are not directly bound to fluorines remain close to zero during the C−F bond oscillation, as determined by the DFT calculations. This lack of electronic polarization can be explained by the quasi one-dimensional structure of SWNTs, together with the fact that SWNT walls are made of a single atomic layer. The C−F vibrations excited by the IR radiation relax through valence bonding between the fluorine and carbon atoms. The corresponding bonding interactions are significantly weaker between molecules and bulk metal surfaces.

Finally, we should mention the future prospects and limitation of the present studies. Our analysis was based on classical MD with the AMBER potential. Changes in the electronic structure of the sp^2 carbons due to their long-range interactions with the fluorine atoms were not fully taken into account. Such changes may affect the dynamics and polarization of the system. In principle, they can be included

DOI: 10.1021/jz100143z | J. Phys. Chem. Lett. 2010, 1, 1307–1311

by first-principles MD; however, this approach is computationally too expensive for the calculation of the IR spectra. The current analysis focused on the linear IR response function. It allowed us to successfully distinguish the 1,2- and 1,4-strucures. Further information, including coupling between the C−F bonds, structural defects, and locations of boundaries between the 1,2- and 1,4-isomer domains, may be obtained by analysis of nonlinear response functions that are relevant for multidimensional vibrational spectroscopies. [53−56] We leave this for future studies.

In conclusion, our calculations show that the [−C(sp^3)−C(sp^3)−] collective vibrational peak is observed at 400 cm^{-1} only in the IR spectrum of the 1,2-fluorine addition structure, whereas the F−C(sp^3) stretching motion coupled with neighboring C(sp^2) atoms is observed at 1300 cm^{-1} only in the 1,4-addition structure for light polarized along the tube axis. These predicted spectral differences create a possibility to distinguish between the different F-SWNT isomers using IR measurements. Furthermore, if the 1,2- and 1,4-addition structures coexist, their ratio can be determined by the relative intensities of the spectral peaks associated with each structure.

AUTHOR INFORMATION

Corresponding Author:

*To whom correspondence should be addressed.

ACKNOWLEDGMENT The authors thank Tammie Nelson for comments on the manuscript. A.U. is supported by the research fellowship of the Global COE Program, International Center for Integrated Research, and Advanced Education in Material Science, Kyoto University. Y.T. is grateful for the financial support in the form of a Grant-in-Aid for Scientific Research B19350011 from the Japan Society for the Promotion of Science. O.V.P. acknowledges the support of the U.S. Department of Energy, Grant #DE-FG02-05ER15755. O.V.P. is a Foreign Scholar of the Japan Society for the Promotion of Science.

REFERENCES

(1) Iijima, S. Helical Microtubules of Graphitic Carbon. *Nature* **1991,** *354*, 56–58.
(2) Kanungo, M.; Lu, H.; Malliaras, G. G.; et al. Suppression of Metallic Conductivity of Single-Walled Carbon Nanotubes by Cycloaddition Reactions. *Science* **2009,** *323*, 234–237.
(3) Lu, J.; Wang, D.; Nagase, S.; et al. Evolution of the Electronic Properties of Metallic Single-Walled Carbon Nanotubes with the Degree of CCl2 Covalent Functionalization. *J. Phys. Chem. B* **2006,** *110*, 5655–5658.
(4) Bachilo, S. M.; Strano, M. S.; Kittrell, C.; et al. Structure-Assigned Optical Spectra of Single-Walled Carbon Nanotubes. *Science* **2002,** *298*, 2361–2366.
(5) Strano, M. S.; Dyke, C. A.; Usrey, M. L.; et al. Electronic Structure Control of Single-Walled Carbon Nanotube Functionalization. *Science* **2003,** *301*, 1519–1522.
(6) McPhail, M. R.; Sells, J. A.; He, Z.; et al. Charging Nanowalls: Adjusting the Carbon Nanotube Isoelectric Point via Surface Functionalization. *J. Phys. Chem. C* **2009,** *113*, 14102–14109.
(7) Hayashi, T.; Shimamoto, D.; Kim, Y. A.; et al. Selective Optical Property Modification of Double-Walled Carbon Nanotubes by Fluorination. *ACS Nano* **2008,** *2*, 485–488.
(8) Habenicht, B. F.; Craig, C. F.; Prezhdo, O. V. Time-Domain Ab Initio Simulation of Electron and Hole Relaxation Dynamics in a Single-Wall Semiconducting Carbon Nanotube. *Phys. Rev. Lett.* **2006,** *96*, 187401.
(9) Habenicht, B. F.; Prezhdo, O. V. Nonradiative Quenching of Fluorescence in a Semiconducting Ab Initio Study. *Phys. Rev. Lett.* **2008,** *100*, 197402.
(10) Habenicht, B. F.; Kamisaka, H.; Yamashita, K.; et al. Ab Initio Study of Vibrational Dephasing of Electronic Excitations in Semiconducting Carbon Nanotubes. *Nano Lett.* **2007,** *7*, 3260–3265.
(11) Yarotski, D. A.; Kilina, S. V.; Talin, A. A.; et al. Scanning Tunneling Microscopy of DNA-Wrapped Carbon Nanotubes. *Nano Lett.* **2009,** *9*, 12–17.
(12) Murakoshi, K.; Okazaki, K. Electrochemical Potential Control of Isolated Single-Walled Carbon Nanotubes on Gold Electrobe. *Electrochim. Acta* **2005,** *50*, 3069–3075.
(13) Takeda, N.; Murakoshi, K. Characteristics of the Raman Spectra of Single-Walled Carbon Nanotube Bundles under Electrochemical Potential Control. *Anal. Bioanal. Chem.* **2007,** *388*, 103–108.
(14) Liu, Z.; Tabakman, S. M.; Chen, Z.; et al. Preparation of Carbon Nanotube Bioconjugates for Biomedical Applications. *Nature Protocols* **2009,** *4*, 1372–1382.
(15) Satishkumar, B. C.; Brown, L. O.; Gao, Y.; et al. Reversible Fluorescence Quenching in Carbon Nanotubes for Biomolecular Sensing. *Nat. Nanotechnol.* **2007,** *2*, 560–564.
(16) Barone, P. W.; Baik, S.; Heller, D. A.; et al. Near-Infrared Optical Sensors Based on Single-Walled Carbon Nanotubes. *Nat. Mater.* **2005,** *4*, 86–92.
(17) Li, S. S.; He, H.; Jiao, Q. C.; et al. Applications of Carbon Nanotubes in Drug and Gene Delivery. *Prog. Chem.* **2008,** *20*, 1798–1803.
(18) Zhang, Y. Y.; Stan, L.; Xu, P.; et al. A Double-Layered Carbon Nanotube Array with Super-Hydrophobicity. *Carbon* **2009,** *47*, 3332–3336.
(19) Kakade, B. A.; Pillai, V. K. Tuning the Wetting Properties of Multiwalled Carbon Nanotubes by Surface Functionalization. *J. Phys. Chem. C* **2008,** *112*, 3183–3186.
(20) Usrey, M. L.; Strano, M. S. Controlling Single-Walled Carbon Nanotube Surface Adsorption with Covalent and Noncovalent Functionalization. *J. Phys. Chem. C* **2009,** *113*, 12443–12453.
(21) Pulikkathara, M. X.; Kuznetsov, O. V.; Peralta, I. R. G..; et al. Medium Density Polyethylene Composites with Functionalized Carbon Nanotubes. *Nanotechnology* **2009,** *20*, 195602.
(22) Thomas, P.; Himmel, D.; Mansot, J. L.; et al. Tribological Properties of Fluorinated Carbon Nanofibres. *Tribology Lett.* **2009,** *34*, 49–59.
(23) Sato, Y.; Ootsubo, M.; Yamamoto, G.; et al. Super-Robust, Lightweight, Conducting Carbon Nanotube Blocks Cross-Linked by De-Fluorination. *Acs Nano* **2008,** *2*, 348–356.
(24) Kalugin, O. N.; Chaban, V. V.; Loskutov, V. V.; et al. Uniform Diffusion of Acetonitrile Inside Carbon Nanotubes Favors Supercapacitor Performance. *Nano Lett.* **2008,** *8*, 2126–2130.
(25) Groult, H.; Nakajima, T.; Tressaud, A.; et al. Opening Mechanism of Closed Graphitized Tips via Low-Temperature Surface Fluorination. *Electrochem. Solid State Lett.* **2007,** *10*, A212–A215.

DOI: 10.1021/jz100143z | *J. Phys. Chem. Lett.* **2010,** *1*, 1307–1311

(26) Hattori, Y.; Noguchi, N.; Okino, F.; et al. Defluorination-Enhanced Hydrogen Adsorptivity of Activated Carbon Fibers. *Carbon* **2007,** *45*, 1391–1395.
(27) Casey, J. P.; Bachilo, S. M.; Weisman, R. B. Efficient Photosensitized Energy Transfer and Near-IR Fluorescence from Porphyrin−SWNT Complexes. *J. Mater. Chem.* **2008,** *18*, 1510–1516.
(28) Tasis, D.; Tagmatarchis, N.; Bianco, A.; et al. Chemistry of Carbon Nanotubes. *Chem. Rev.* **2006,** *106*, 1105–1136.
(29) Lee, Y. S. Syntheses and Properties of Fluorinated Carbon Materials. *J.Fluorine Chem.* **2007,** *128*, 392–403.
(30) Nakajima, T. *Fluorine−Carbon and Fluoride−Carbon Materials*; Marcel Dekker, Inc.: New York, 1995.
(31) Mickelson, E. T.; Huffman, C. B.; Rinzler, A. G.; et al. Fluorination of Single-Wall Carbon Nanotubes. *Chem. Phys. Lett.* **1998,** *296*, 188–194.
(32) da Silva, A. M.; Junqueira, G. M. A.; Anconi, C. P. A.; et al. New Insights on Chemical Oxidation of Single-Wall Carbon Nanotubes: A Theoretical Study. *J. Phys. Chem. C* **2009,** *113*, 10079–10084.
(33) Alemany, L. B.; Zhang, L.; Zeng, L. L.; et al. Solid-State NMR Analysis of Fluorinated Single-Walled Carbon Nanotubes: Assessing the Extent of Fluorination. *Chem. Mater.* **2007,** *19*, 735–744.
(34) Zurek, E.; Pickard, C. J.; Autschbach, J. A Density Functional Study of the C-13 NMR Chemical Shifts in Fluorinated Single-Walled Carbon Nanotubes. *J. Phys. Chem. A* **2009,** *113*, 4117–4124.
(35) Kelly, K. F.; Chiang, I. W.; Mickelson, E. T.; et al. Insight into the Mechanism of Sidewall Functionalization of Single-Walled Nanotubes: An STM Study. *Chem. Phys. Lett.* **1999,** *313*, 445–450.
(36) Hayashi, T.; Terrones, M.; Scheu, C.; et al. Nano Teflons: Structure and EELS Characterization of Fluorinated Carbon Nanotubes and Nanofibers. *Nano Lett.* **2002,** *2*, 491–496.
(37) An, K. H.; Heo, J. G.; Jeon, K. G.; et al. X-ray Photoemission Spectroscopy Study of Fluorinated Single-Walled Carbon Nanotubes. *Appl. Phys. Lett.* **2002,** *80*, 4235–4237.
(38) Plank, N. O. V.; Cheung, R. Functionalisation of Carbon Nanotubes for Molecular Electronics. *Microelecton. Eng.* **2004,** *73−74*, 578–582.
(39) Bettingner, H. F. Experimental and Computational Investigations of the Properties of Fluorinated Single-Walled Carbon Nanotubes. *ChemPhysChem* **2003,** *4*, 1283–1289.
(40) Ewels, C. P.; Van Lier, G.; Charlier, J. C.; et al. Pattern Formation on Carbon Nanotube Surfaces. *Phys. Rev. Lett.* **2006,** *96*, 216103.
(41) Kudin, K. N.; Bettingner, H. F.; Scuseria, G. E. Fluorinated Single-Wall Carbon Nanotubes. *Phys. Rev. B* **2001,** *63*, 045413.
(42) Shiomi, J.; Maruyama, S. Non-Fourier Heat Conduction in a Single-Walled Carbon Nanotube: Classical Molecular Dynamics Simulations. *Phys. Rev. B* **2006,** *73*, 205420.
(43) Shiomi, J.; Maruyama, S. Molecular Dynamics of Diffusive-Ballistic Heat Conduction in Single-Walled Carbon Nanotubes. *Jpn.J.Appl.Phys.* **2008,** *47*, 2005–2009.
(44) Yang, S.; Cho, M. Thermal Denaturation of Polyalanine Peptide in Water by Molecular Dynamics Simulations and Theoretical Prediction of Infrared Spectra: Helix-Coil Transition Kinetics. *J. Phys. Chem. B* **2007,** *111* (3), 605–617.
(45) Kwac, K.; Lee, K. K.; Han, J. B.; et al. Classical and Quantum Mechanical/Molecular Mechanical Molecular Dynamics Simulations of Alanine Dipeptide in Water: Comparisions with IR and Vibrational Circular Dichroism Spectra. *J. Chem. Phys.* **2008,** *128*, 105106.
(46) Bursulaya, B. D.; Kim, H. J. Spectroscopic and Dielectric Properties of Liquid Water: A Molecular Dynamics Simulation Study. *J. Chem. Phys.* **1998,** *109*, 4911–4919.
(47) Saito, S.; Ohmine, I. Third Order Nonlinear Response of Liquid Water. *J. Chem. Phys.* **1997,** *106*, 4889–4893.
(48) Rao, A. M.; Richter, E.; Bandow, S.; et al. Diameter-Selective Raman Scattering from Vibrational Modes in Carbon Nanotubes. *Science* **1997,** *275*, 187–191.
(49) Mukamel, S. *Principles of Nonlinear Optical Spectroscopy*; Oxford University Press: New York, 1995.
(50) Cornell, W. D.; Cieplak, P.; Bayly, Cl.; et al. A Second Generation Force Field for the Simulation of Proteins, Nucleic Acids, and Organic Molecules. *J. Am. Chem. Soc.* **1995,** *117*, 5179–5197.
(51) Claves, D.; Rossignol, J. Fluorine Addition to Single-Wall Carbon Nanotubes Revisited. *Chem. Phys. Lett.* **2009,** *468*, 231–233.
(52) Tully, J. C.; Gomez, M.; Headgordon, M. Electronic and Phonon Mechanisms of Vibrational-Relaxation — CO on Cu(100). *J. Vac. Sci. Technol. A* **1993,** *11*, 1914–1920.
(53) Tanimura, Y.; Mukamel, S. Two-Dimensional Femtosecond Vibrational Spectroscopy of Liquids. *J. Chem. Phys.* **1993,** *99* (12), 9496–9511.
(54) Nagata, Y.; Tanimura, Y.; Mukamel, S. Two-Dimensional Infrared Surface Spectroscopy for CO on Cu(100): Detection of Intermolecular Coupling of Adsorbates. *J. Chem. Phys.* **2007,** *126*, 204703.
(55) Hasegawa, T.; Tanimura, Y. Nonequilibrium Molecular Dynamics Simulations with a Backward−Forward Trajectories Sampling for Multidimensional Infrared Spectroscopy of Molecular Vibrational Modes. *J. Chem. Phys.* **2008,** *128*, 064511.
(56) Tanimura, Y.; Ishizaki, A. Modeling, Calculating, and Analyzing Multidimensional Vibrational Spectroscopies. *Acc. Chem. Res.* **2009,** *42*, 1270–1279.

DOI: 10.1021/jz100143z | *J. Phys. Chem. Lett.* **2010,** *1*, 1307–1311